Continental Shelf Research 231 (2021) 104611

Contents lists available at ScienceDirect

Continental Shelf Research

journal homepage: www.elsevier.com/locate/csr

Mixed layer depth climatology over the northeast U.S. continental shelf (1993–2018)

Cassia Cai [a], Young-Oh Kwon [b,*], Zhuomin Chen [b], Paula Fratantoni [c]

[a] Department of Earth and Planetary Sciences, Northwestern University, Evanston, IL, United States
[b] Department of Physical Oceanography, Woods Hole Oceanographic Institution, Woods Hole, MA, United States
[c] NOAA Fisheries, Northeast Fisheries Science Center, National Marine Fisheries Service, Woods Hole, MA, United States

A R T I C L E I N F O

Keywords:
Mixed layer depth
Northeast U.S. continental shelf
Climatology

A B S T R A C T

The Northeast U.S. (NEUS) continental shelf has experienced rapid warming in recent decades. Over the NEUS continental shelf, the circulation and annual cycle of heating and cooling lead to local variability of water properties. The mixed layer depth (MLD) is a key factor that determines the amount of upper ocean warming. A detailed description of the MLD, particularly its seasonal cycle and spatial patterns, has not been developed for the NEUS continental shelf. We compute the MLD using an observational dataset from the Northeast Fisheries Science Center hydrographic monitoring program. The MLD exhibits clear seasonal cycles across five eco-regions on the NEUS continental shelf, with maxima in January–March and minima in July or August. The seasonal cycle is largest in the western Gulf of Maine (71.9 ± 24.4 m), and smallest in the southern Mid-Atlantic Bight (34.0 ± 7.3 m). Spatial variations are seasonally dependent, with greatest homogeneity in summer. Interannual variability dominates long-term linear trends in most regions and seasons. To evaluate the sensitivity of our results, we compare the MLDs calculated using a 0.03 kg/m^3 density threshold with those using a 0.2 °C temperature threshold. Temperature-based MLDs are generally consistent with density-based MLDs, although a small number of temperature-based MLDs are biased deep compared to density-based MLDs particularly in spring and fall. Finally, we compare observational MLDs to the MLDs from a high-resolution ocean reanalysis GLORYS12V1. While the mean values of GLORYS12V1 MLDs compare well with the observed MLDs, their interannual variability are not highly correlated, particularly in summer. These results can be a starting point for future studies on the drivers of temporal and spatial MLD variability on the NEUS continental shelf.

1. Introduction

The Northeast U.S. (NEUS) continental shelf, which supports some of the world's most productive and commercially valuable fisheries, has experienced significant changes in recent decades exacerbating the effect of long-term warming. The warming trend and intermittent extreme events have significant impacts on the marine ecosystem, including driving changes in species distributions and abundance (Nye et al., 2009, 2011; Mills et al., 2013; Pershing et al., 2015).

Shearman and Lentz (2010) analyzed long-term sea-surface temperature (SST) trends along the U.S. East Coast for 1875–2007 based on observations from lighthouses and lightships, finding a warming trend of ~0.7–1.0 °C per century along the NEUS coast. Chen et al. (2020) found a consistent warming rate for the period 1900–2018 across the entire shelf from the NEUS to the Labrador Sea. In addition, they showed that the warming rate has accelerated in recent decades, estimating a rate of ~0.37 °C per decade in 1982–2018. They suggested that approximately two thirds of the recent accelerated warming could be attributed to natural multidecadal variability while the rest is likely externally forced, including via anthropogenic warming. Harden et al. (2020) reported that summer temperatures measured between 2003 and 2013 across the New England shelfbreak south of Cape Cod have increased at an overall rate of 0.58 °C per decade. Most of the observed warming occurred in the upper 20 m, resulting in decreases in near-surface density and nearly two-fold increases in stratification. On the other hand, Forsyth et al. (2015) examined temperature measurements collected between 1977 and 2013 along the CMV Oleander section crossing the continental shelf and slope offshore of New Jersey, showing that enhanced warming is concentrated near the shelfbreak but penetrates the entire water column, implying a critical role of the shelfbreak front. They reported that

* Corresponding author. Physical Oceanography Department, Woods Hole Oceanographic Institution, MS#21, Woods Hole, MA, 02543, United States.
E-mail address: yokwon@whoi.edu (Y.-O. Kwon).

https://doi.org/10.1016/j.csr.2021.104611
Received 7 May 2021; Received in revised form 25 September 2021; Accepted 2 November 2021
Available online 8 November 2021

depth-averaged warming trends in 2002–2013 were more than five times those recorded between 1977 and 2001.

In addition to regional warming trends, a number of notable extreme warming events have been reported. One example is the marine heat wave observed in 2012 in which SST measured 1–3 °C warmer than baseline conditions (Mills et al., 2013; Chen et al., 2015). Anomalous jet stream variability was suggested as the main driver of this event (Chen et al., 2014). Extreme heat waves are not only confined to the surface ocean. For example, Gawarkiewicz et al. (2012) reported bottom temperature anomalies greater than 6 °C in November 2011 near the Mid-Atlantic Bight shelfbreak, attributed to a large meander in the Gulf Stream path. Further, Gawarkiewicz et al. (2019) examined an advective event in the Mid-Atlantic Bight near the end of 2016, associated with a large Gulf Stream Warm Core Ring. Here, depth averaged temperature anomalies measuring ~6 °C and salinity anomalies of ~1 psu propagated equatorward along the shelf from New England to Cape Hatteras over the course of ~4 months.

The NEUS continental shelf is characterized by contrasting water masses, resulting in strong horizontal property gradients and persistent thermohaline fronts (Townsend et al., 2006). The warm and saline northward-flowing Gulf Stream and the colder and fresher southward-flowing Labrador Current converge and interact in this region, forming the source waters for the continental shelf (Loder et al., 1998; Fratantoni and Pickart, 2007; Greene et al., 2013; Richaud et al., 2016). The surface layers are dominated by shelf waters entering the Gulf of Maine (GoM) from the north, while deeper layers are sourced by a mixture of slope waters from the north and south entering the GoM through the Northeast Channel (Mountain and Manning, 1994; Mountain and Taylor, 1998; Mountain, 2012). The shelf circulation and annual cycle of heating, along with influxes of freshwater from riverine sources, result in local variability of water properties.

The NEUS continental shelf consists of 5 eco-regions, which are impacted by the changing climate in non-uniform ways. These include the Western Gulf of Maine (WGOM), Eastern Gulf of Maine (EGOM), Georges Bank (GB), Northern Mid-Atlantic Bight (NMAB), and Southern Mid-Atlantic Bight (SMAB) (Fig. 1). The unique geography of the NEUS continental shelf, along with its considerable regional variations in

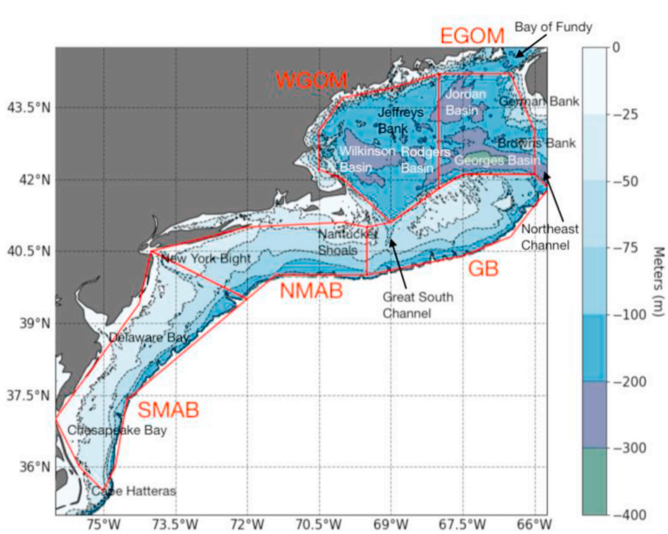

Fig. 1. Map of the Northeast U.S. continental shelf and the five eco-regions defined by the NOAA Northeast Fisheries Science Center Ecosystem Assessment Program: Southern Mid-Atlantic Bight (SMAB), Northern Mid-Atlantic Bight (NMAB), Georges Bank (GB), Western Gulf of Maine (WGOM), and Eastern Gulf of Maine (EGOM). In addition, the major bathymetric and geographical features are noted. Bathymetric contours at 25, 75, 100, 200, 300, and 400 m are plotted based on the ETOPO1 dataset (Amante and Eakins, 2009).

temperature, salinity, bathymetry, and geometry, complicates the study of its subsurface features (Townsend et al., 2006; Richaud et al., 2016; Bisagni et al., 2016). One such feature is the mixed layer, within which density is almost vertically uniform. A study of the mixed layer is particularly important for this region as its thickness, or the mixed layer depth (MLD), is one of the key factors that determines the amount of warming experienced in the upper ocean (Alexander et al., 2018). To our knowledge, a detailed description of the MLD and particularly its seasonal cycle has not been constructed for the entire NEUS continental shelf. Available global MLD climatologies (e.g., de Boyer Montegut, 2004) are typically too coarse to resolve details in the coastal ocean.

In the absence of a regional MLD dataset for the NEUS continental shelf, previous heat budget studies have been forced to either consider the full water column instead of the mixed layer (e.g., Chen et al., 2014) or to estimate the MLD using a diagnostic mixed layer model (e.g., Chen and Kwon, 2018). When the MLD is treated as a constant in time and/or space in heat budget calculations, the relative role of the various drivers of SST or upper ocean heat content can often be misinterpreted. Given a surface heat flux change, the degree or even the sign of the SST change can vary depending on the change in MLD. For example, in an analysis of the mixed layer temperature budget, Yamamoto et al. (2020) found that MLD changes can influence Atlantic multidecadal variability (AMV). In particular, the AMV warm phase is linked to the deepening of the MLD, which increases the ocean heat capacity (Yamamoto et al., 2020).

The mixed layer is created through vigorous turbulent processes, including wind forcing, evaporation, sea ice formation, and internal mixing (Niiler, 1975; Alexander et al., 2000). Typically, in spring and summer, weak wind stress and strong atmospheric heating at the surface result in a sharp thermocline and shallow mixed layer. As wind stress increases and the atmosphere cools the ocean in fall and winter, stratification weakens which leads to the development of deeper mixed layers. Freshwater transport, lateral advection of heat, near-surface salinity changes, and the presence of fronts, among others, can influence both the timing and strength of stratification. Moreover, stratification can be dominated by temperature, salinity, or a combination of both (Li et al., 2015). The processes affecting upper ocean mixing and stratification exhibit strong seasonal and spatial variations on the NEUS continental shelf. For example, GB is subject to weak stratification throughout the year as a result of persistent tidal mixing, while the GoM exhibits seasonal variations in stratification with phase and amplitude that vary from east to west (Loder et al., 1998; Mountain and Manning, 1994; Li et al., 2015). Therefore, the MLD is expected to exhibit strong seasonal cycles and spatial inhomogeneity across the NEUS continental shelf.

The identification of MLD in *in situ* hydrographic data is not a trivial task, due to often limited vertical resolution, instrument noise, and/or fine scale physical variability in the upper ocean. As a consequence, numerous definitions have been proposed for application to the upper ocean (e.g., de Boyer Montegut, 2004; Thomson and Fine, 2003; Holte and Talley, 2009). For instance, the mixed layer has been defined based on the vertical variation of temperature and density, and the two most common approaches are the threshold method and the gradient method. In the threshold method, the temperature or density at each subsurface depth is compared with a surface reference value until a depth is reached where the difference exceeds a threshold value. Alternatively, the gradient method locates the base of a mixed layer in profiles by searching for the depth at which a specified gradient value is exceeded. This method relies on the fact that profiles of temperature and density typically include sharp gradients at the base of the mixed layer. Thus, the threshold method is often preferred over the gradient method since observed profiles are typically noisy as a result of turbulent mechanical mixing and instrument noise. de Boyer Montégut et al. (2004) built an MLD climatology for the global ocean from 4 million individual profiles, determining that the most appropriate thresholds are 0.03 kg/m^3 for density and 0.2 °C for temperature relative to a reference depth of 10 m. Holte and Talley (2009) use a combination of the gradient method and the threshold method to calculate candidate MLD values from different methods, objectively comparing the results to determine the final MLD from each profile. Here we use the most common and simplest scheme, the threshold method, for finding the MLD, considering the noisy observational vertical profiles in the NEUS coastal ocean. The density threshold is preferred over the temperature threshold because the degree of turbulent mixing is influenced directly by the density structure (Holte and Talley, 2009). Moreover, in coastal environments, haline controls on stratification can be large locally, thus the temperature- and density-based MLDs can be different (e.g. Christensen and Pringle, 2012).

The primary goal of this study is to investigate the seasonal cycle of MLD across the entire NEUS shelf. We compare mixed layers derived from an *in situ* observational dataset maintained by NOAA's Northeast Fisheries Science Center (NEFSC) with those calculated from an eddy-resolving ocean reanalysis dataset from the GLobal Ocean ReanalYsis and Simulation project (GLORYS12V1). The objectives of this study are threefold: (1) to describe the MLD seasonal cycle across the entire NEUS shelf, (2) to investigate the long-term change in MLD over the period spanning 1993 to 2018, and (3) to assess the GLORYS12V1 ocean reanalysis dataset against *in situ* estimates.

The outline of this paper is as follows. The observational and reanalysis datasets are described in detail in Section 2. In addition, two threshold methods for determining MLD are described (based on density and temperature, respectively). In Section 3, the observed mean seasonal evolution and spatial patterns of the density-based MLDs are presented, along with their long-term variability and trends. A comparison between density-based and temperature-based MLDs is also presented in Section 3. In Section 4, we identify differences between the density-based MLDs calculated from *in situ* observations and GLORYS12V1. Discussions and conclusions are presented in Section 5.

2. Data and methods

2.1. The NEFSC hydrographic dataset

The NEFSC collects hydrographic data from regionally-focused and shelf-wide surveys several times each year (Fratantoni et al., 2019). Here, the study period (1993–2018) was chosen because the availability of profile data collected via CTD instruments is low prior to 1992 and this period covers the same altimetry era by GLORYS12v1. The spatial and temporal distribution of data is uneven (Fig. 2). Spring (March–May) and fall (September–November) are the two most data-abundant seasons, containing 12,607 and 11,613 profiles, respectively. Observations are sparse in winter (4795 profiles), particularly in December. In recent years, there has been a decline in seasonal and spatial coverage. Spatially, observations are most abundant in the GB eco-region (12,363 profiles), followed by the SMAB (9581 profiles), WGOM (6838 profiles), NMAB (5684 profiles), and EGOM (3874 profiles) regions. Note that the NEFSC survey does not sample inshore of 15 m isobath.

2.2. GLORYS12V1 ocean reanalysis

The GLORYS12V1 product is a data-assimilated eddy-resolving global reanalysis (1/12° horizontal resolution and 50 vertical levels), publicly available from the Copernicus Marine Environment Monitoring Service. Observations such as *in situ* temperature and salinity profiles, satellite SST, and along-track sea-level anomalies from satellite altimetry, are assimilated to simulate the evolution of the physical ocean properties. The data assimilation method used is a reduced-order Kalman filter. The numerical model used is the Nucleus for European Modelling of the Ocean (NEMO) general circulation model with model surface boundary conditions derived from the European Centre for Medium-Range Weather Forecasts (ECMWF) atmospheric reanalysis and forecasts. An evaluation of the model acknowledges some drift at depth due to the lack of an accurate interior mixing scheme and model tuning (Drillet et al., 2014; Lellouche et al., 2018).

The GLORYS12V1 product includes an MLD variable, calculated using a variable density threshold corresponding to a 0.2 °C temperature decrease relative to the temperature at 10 m depth (Fernandez and Lellouche, 2018). The climatological GLORYS12V1 density threshold is reproduced as a range of density thresholds by month, which has a distinct seasonal cycle ranging from ~0.025 kg/m^3 in January–April to ~0.05 kg/m^3 in July–September (Fig. 3). In addition to the MLD values provided by the GLORYS12V1 (hereafter GMLD), we also directly calculate MLDs from a subset of GLORYS12V1 daily temperature and salinity profiles extracted at time and space points nearest to observed NEFSC stations, using the density-based criterion described in Section 2.3. We refer to these directly calculated MLDs as GMLD03. The comparison between GMLD03 and GMLD reveals the sensitivity to the MLD definition.

2.3. Determining the MLD

The MLD is determined from each profile in the NEFSC hydrographic database using a finite difference criterion, specifically a density threshold value of 0.03 kg/m^3 measured relative to the mean surface layer density (de Boyer Montegut, 2004). The surface layer includes the top 5 m of the water column. Starting at the bottom of the surface layer (i.e., 5 m depth), the algorithm calculates the potential density change at

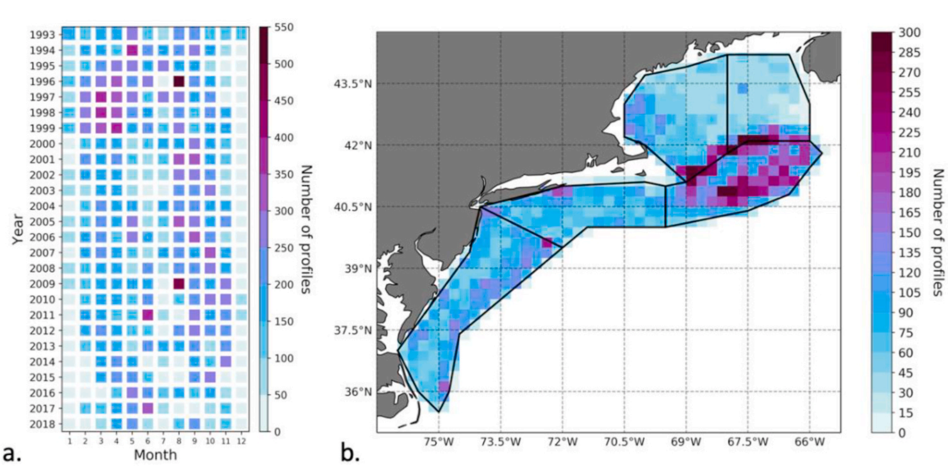

Fig. 2. Temporal and Spatial coverage of the observational profiles from NEFSC. **(a)** Monthly data coverage from 1993 to 2018 on the NEUS continental shelf from the NEFSC hydrographic dataset and **(b)** spatial distribution of number of profiles within each 0.25° × 0.25° bin (horizontal resolution) from 1993 to 2018 of all seasons compiled together. The black lines indicate the boundaries for the 5 eco-regions shown in Fig. 1.

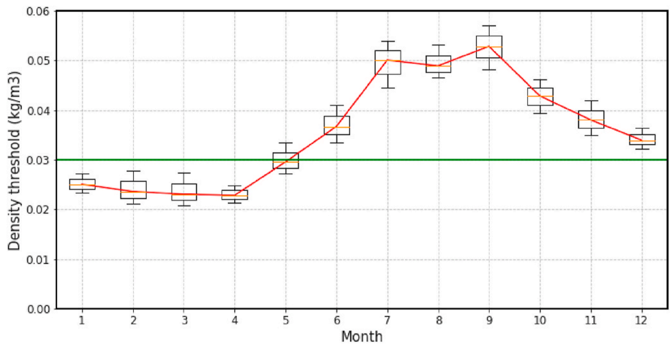

Fig. 3. Boxplot showing the climatological distribution of density threshold used in GLORYS12V1 by month corresponding to a 0.2 °C temperature decrease from the reference temperature value at 10 m. The green line specifies the 0.03 kg/m^3 density threshold. The average of the median density thresholds by month used in GLORYS12V1 is 0.036 kg/m^3.

each progressively deeper depth. At the first instance where the density differs from the mean surface layer density by the threshold value or greater, the algorithm terminates the search, and that depth is identified as the MLD.

This method of MLD detection results in four categories (Fig. 4): (a) a well-defined mixed layer within the profile, above which the density is relatively uniform and below which density is stratified, (b) a fully mixed profile where the MLD is detected within the bottom layer, (c) a fully-stratified profile where the MLD is detected at 5 m, and (d) an inconclusive profile, where the MLD is undetected, and the deepest measurement is not within the bottom layer. For profiles that have a sea floor depth of 25 m or shallower, the bottom layer is defined as the bottom 5 m of the water column. For profiles that have a sea floor depth greater than 25 m, the bottom layer is defined as the bottom 10 m of the water column. The profiles falling in category (c), i.e. the fully stratified profiles, are assigned with the MLD values of 5 m, while those in category (d) are not considered to have a known MLD and thus are excluded from further analyses. The MLD for profiles in the second category (b) are set equal to the sea floor depth.

Temperature-based MLDs are determined using a similar threshold method with a finite temperature difference criterion of 0.2 °C relative to the surface (top 5 m average) value (de Boyer Montegut, 2004). Using the temperature-based MLD detection scheme, 62.1% of all profiles have well-defined MLDs, 22.5% are fully-mixed, 9.5% are fully-stratified, and 5.9% are inconclusive. Compared to the MLDs detected using the 0.03 kg/m^3 density threshold, the temperature threshold criteria yields fewer fully stratified profiles (by 6.9%) and more fully mixed (by 6.1%) and well-defined MLD (by 0.6%) ones. The fact that fewer fully stratified profiles resulting from the temperature threshold criteria suggests that the very shallow mixed layers are driven by salinity stratification associated with a fresh surface layer (e.g. Christensen and Pringle, 2012). Of the 38,340 total profiles, the density threshold method results in 36,173 profiles (94.3%) with MLD values assigned. On the other hand, the temperature threshold method results in 36,072 such profiles (94.1%). An example of a profile where the temperature-based MLD differs from the density-based MLD is shown in Fig. 5.

3. Observed seasonal cycle and long-term variability

3.1. Mean seasonal evolution and spatial patterns of MLDs using density-based criterion

In all 5 eco-regions, the climatological mean MLDs using the 0.03 kg/m^3 density-based criteria exhibit clear seasonal cycles with maxima in January–March and minima in July or August (Fig. 6). Regional differences are prominent and primarily found in winter where the deepest MLDs range from 40.7 ± 6.3 m in the SMAB to 78.5 ± 22.9 m in the WGOM. (Note that one standard deviation is used as the uncertainty range throughout this paper.) In summer, regional differences are relatively small for the shallowest mean MLD, ranging from 6.1 m to 8.3 m in all regions. The amplitude of the seasonal cycle is largest in the WGOM, ranging from 78.5 ± 22.9 m in January when the upper layers of the WGOM are strongly mixed, to 6.5 ± 1.5 m in July when stratification dominates. The seasonal cycle is less pronounced in GB and the SMAB, where the annual range is 35.8 ± 17.3 m (max: 42.8 ± 15.6 m and min: 7.0 ± 1.7 m) and 34.0 ± 7.3 m (max: 40.7 ± 6.3 m and min: 6.7 ± 1.0 m), respectively. This is not surprising as GB typically remains mixed throughout the year, primarily due to strong tidal mixing (Loder et al., 1993). On the other hand, the smaller seasonal cycle in the SMAB is due to the shallow bathymetry, which limits the winter MLD. The amplitudes of the seasonal cycle in the EGOM and NMAB are 37.2 ± 11.6 m (max: 45.5 ± 8.2 m and min: 8.3 ± 3.4 m) and 41.9 ± 12.6 m (max: 48.0 ± 11.8 m and min: 6.1 ± 0.8 m), respectively. The coastal regions in the MAB, which are generally shallower than 100 m, are very different from the deeper basins in GOM. The seasonal cycle of MLD in the NMAB and SMAB are similar and have comparable amplitudes. The seasonal variation of the standard deviation (STD) is similar to the seasonal cycle of MLD in each region, with STDs peaking in winter and decreasing in spring reaching minimum values in summer before stratification breaks

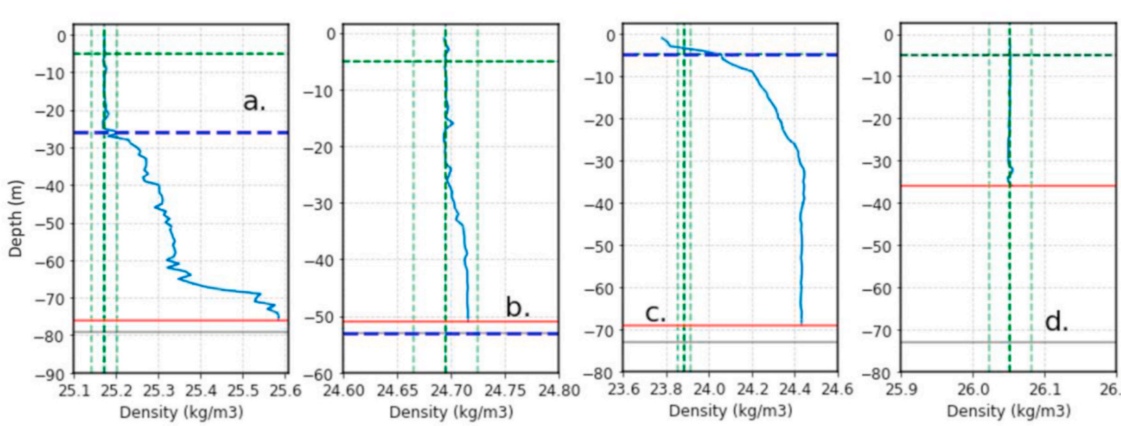

Fig. 4. Examples of the four MLD categories based on the density-threshold MLD detection scheme: **(a)** a well-defined mixed layer within the profile (61.5% of all profiles), **(b)** a fully mixed profile (16.4%), **(c)** a fully stratified profile (16.4%), and **(d)** an inconclusive profile (5.7%). The red line specifies the depth of the deepest observational measurement. The gray line shows the sea floor depth. The dark blue dashed line indicates the detected MLD. The dark green dashed vertical and horizonal lines show the surface layer density value and the 5-m depth mark, respectively. The light green dashed vertical lines designate the density threshold, i.e., 0.03 kg/m^3, from the surface layer density value. In (b), the sea floor depth is considered as the MLD.

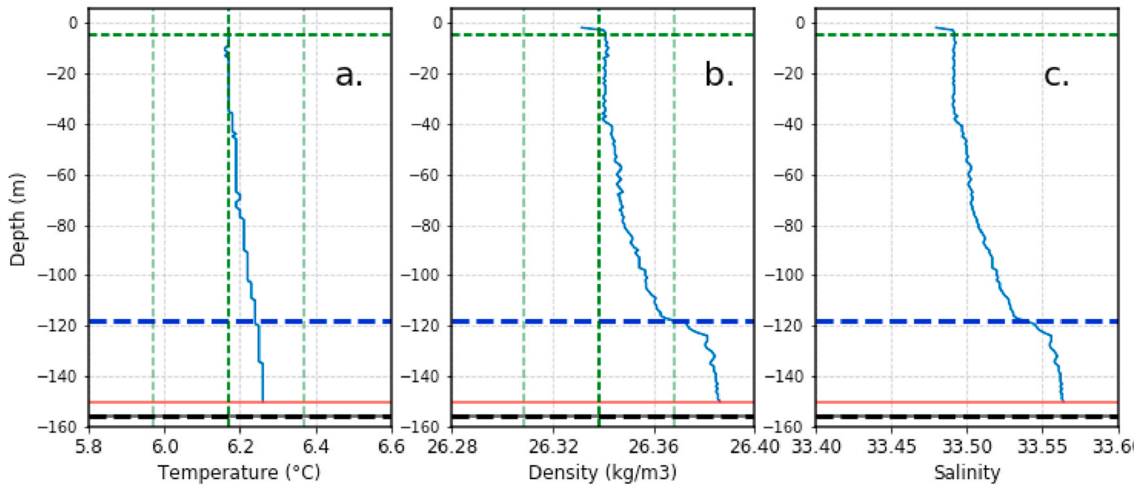

Fig. 5. An example of **(a)** temperature, **(b)** density, and **(c)** salinity profiles where the temperature-based MLD differs from the density-based MLD. This profile was collected at 41.46°N, 69.17°W near the Great South Channel, 2003-01-30. The profile is fully mixed based on the temperature-based detection. The black dashed line shows the temperature-based MLD at 156 m, which is also the sea floor depth, while the blue dashed line shows the density-based MLD at 118 m. In order for the density threshold method to detect the MLD at the bottom (as in the temperature-based case), the density threshold would need to be increased to 0.05 kg/m^3.

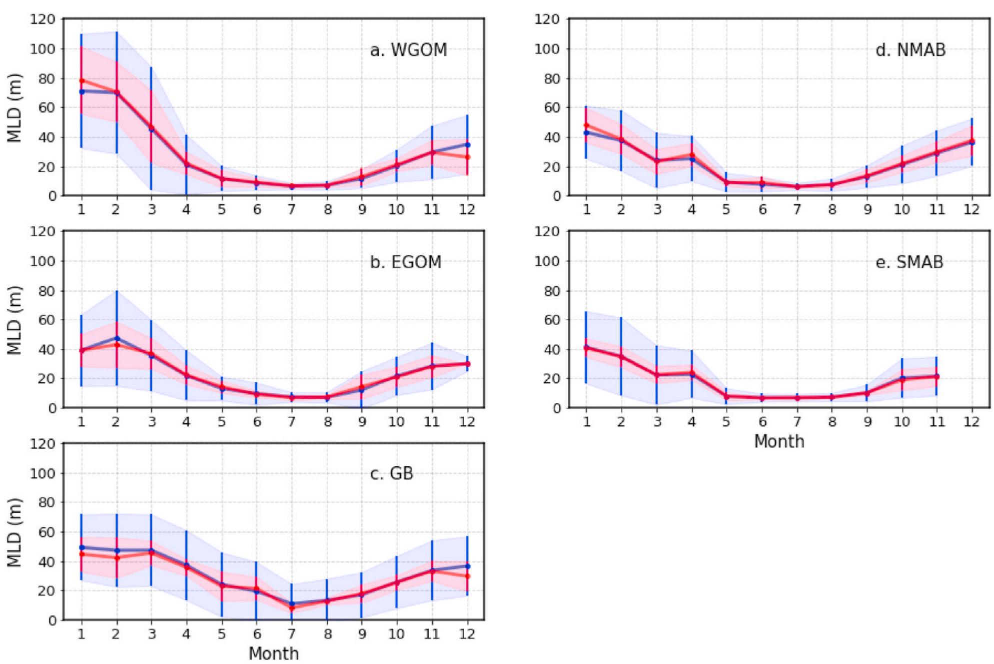

Fig. 6. MLD climatological seasonal cycle from *in situ* observations using density threshold with the 1 standard deviation (STD) ranges shaded, for each eco-region: **(a)** WGOM, **(b)** EGOM, **(c)** GB, **(d)** NMAB, and **(e)** SMAB. For the red curves and shading, the regional mean MLDs are calculated first for each month/year, and monthly means and STDs are calculated subsequently so that the red shading primarily reflects interannual variations. The blue curves and shading are calculated using all data in the region and month at once, therefore also including the variability introduced by variations in the spatial data coverage from year to year. In SMAB, there is no data for December during the study period.

down in fall (Fig. 6). Again, GB is an exception, where the STD is more or less uniform throughout the year.

We further examine the spatial pattern of the MLD seasonal variations in Fig. 7. The greatest seasonal changes are observed in the WGOM. Spatially, MLDs are significantly deeper in the WGOM than in the EGOM in winter while MLD differences between these two eco-regions are not obvious in spring, summer, and fall. MLDs also vary considerably within the WGOM, especially in winter with the deepest mixed layers observed around the Wilkinson Basin especially to the north and south. The deeper mixed layers do not persist into spring. There are also greater spatial MLD differences in NMAB and SMAB during the wintertime, where a cross-shelf MLD gradient is evident with deeper MLDs near the shelf-break, than in other seasons. Overall, there is greater spatial homogeneity in summer, where across the NEUS continental shelf, MLDs are relatively shallow, except for areas on northeast and southwest GB and Nantucket Shoals, likely associated with strong tidal mixing.

The MLD is often limited by the bottom depth over the shallower regions of the NEUS continental shelf, especially in winter when mixing can often extend to the bottom. Thus, some of the regional differences discussed above likely reflect differences in the bathymetry, especially for the differences between the MAB, which is a shallow (<100 m) shelf, and the GOM, which contains deeper basins. As a measure of how much of the water column is occupied by the mixed layer, the ratios between the MLD and bottom depth are calculated (Fig. 8). In winter, the mixed layer almost reaches the bottom in the SMAB, NMAB, and on GB. Hence, the ratio of MLD to total water column depth is greater in these regions than in the WGOM or EGOM. In particular, the entire water column is mixed over parts of GB (shallower than 50 m isobath) throughout the year. As expected, the greatest seasonal change in the ratio is observed in SMAB and NMAB, while WGOM and EGOM exhibit relatively low ratios, which is primarily due to deeper bottom depths in the GoM. This is especially evident in summer, when the mixed layer in the WGOM and

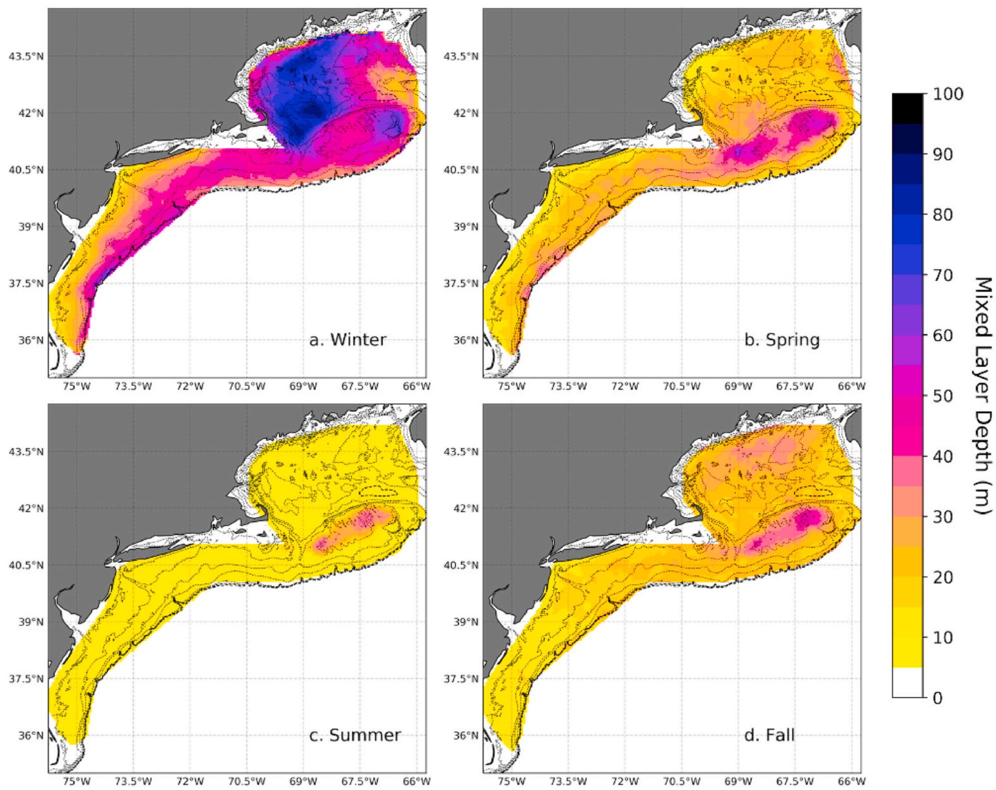

Fig. 7. Spatial patterns of mean MLDs from observations using the density threshold for each season at 0.05-degree resolution: **(a)** winter (December–February), **(b)** spring (March–May), **(c)** summer (June–August), and **(d)** fall (September–November). Bathymetry contours at 25, 50, 75, 100, 200, and 300 m are shown using black dashed lines, and the 300-m contour is thickened.

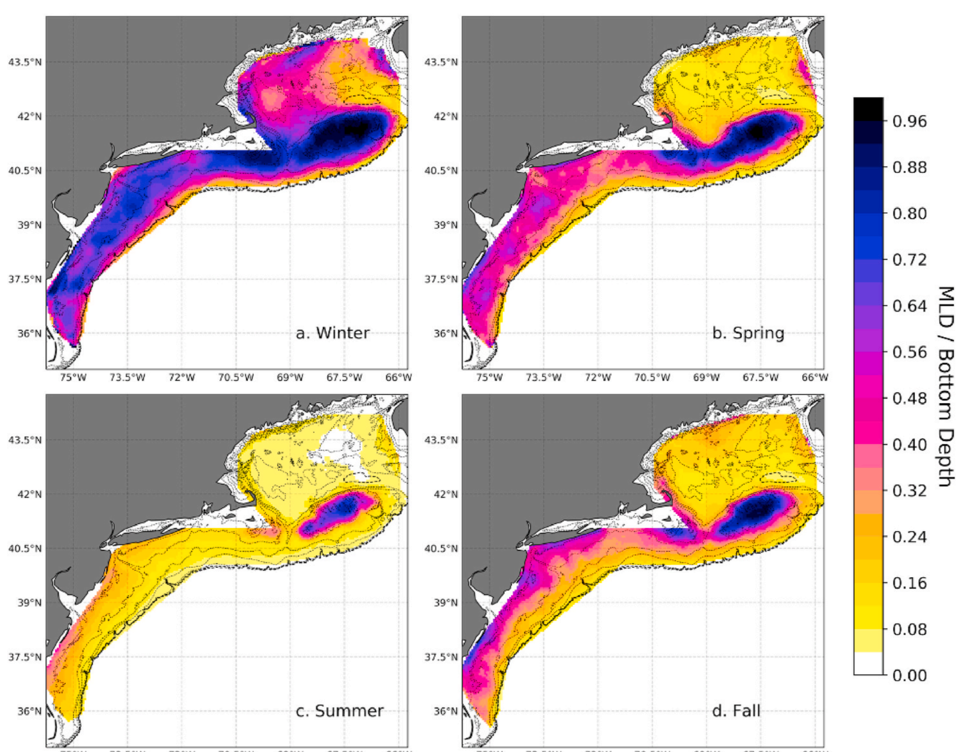

Fig. 8. As in Fig. 7 but showing the mean MLD ratio to bottom depth for each season.

EGOM makes up the smallest portion of the entire water column (6.5 ± 1.3% and 5.9 ± 1.4% in the month with the shallowest MLDs), while mixed layers on GB and in the SMAB occupy a larger portion of the water column (12.2 ± 7.8% and 12.7 ± 4.1% in the month with the shallowest MLDs). When this ratio is averaged over each eco-region (not shown), the greatest seasonal range is observed in the NMAB (60.1%) and GB (58.2%) and smallest in the EGOM (27.7%).

Differences in the amplitude of the seasonal cycle of MLD between the WGOM and EGOM (Figs. 6 and 7) are likely a consequence of the cold, dry air outbreaks experienced in winter off the North American continent. The outbreaks drive intense evaporative heat loss, over the WGOM, thereby producing the deepest winter mixed layers in the region (Brown and Beardsley 1978). As the cold air outbreaks are intermittent, the WGOM is not colder on average than EGOM in the winter climatology (Figs. 9 and 10). Differences can also arise from cross-basin gradients in surface salinity (Figs. 11 and 12; also Richaud et al., 2016, their Fig. 15) which result from the seasonal salinity cycle of the inflowing Scotian Shelf Water and the advection timescales associated with the circulation in the Gulf of Maine (Vermersch et al., 1979; Mountain and Jessen, 1987; Taylor and Mountain, 2009; Bisagni et al., 2016). The mixed layer salinity in the WGOM reaches an annual peak in winter, while the EGOM exhibits relatively lower mixed layer salinity and overall a very weak seasonal cycle. When the surface salinity is high, hence denser, winter cooling is very efficient at driving convective overturning resulting in deeper MLDs.

Almost opposite to the MLD seasonal cycle, the seasonal cycle of mixed layer temperature (MLT) exhibits the minimum spatial gradient in winter and the largest north-south gradient in summer (Figs. 9 and 10). In March, the MLT difference between the WGOM and SMAB is only 2.5 ± 2.1 °C, while it is 6.8 ± 2.9 °C in August. In addition, the cross-shelf MLT gradient in SMAB is strongest in winter and weakest in summer. The mixed layer salinity (MLS) exhibits the largest seasonal cycle in SMAB with maximum salinity in winter (33.3 ± 0.5 psu) and minimum in summer (31.0 ± 0.6 psu) (Fig. 11). The NMAB and WGOM also show the maximum MLS in winter and the minimum in summer, with an amplitude of 1.8 ± 1.6 psu and 1.3 ± 0.8 psu, respectively, while no clear seasonal cycle emerges in the EGOM and GB. In addition to the variations described for the GOM, spatial patterns of MLS (Fig. 12) exhibit large cross-shelf variations in the NMAB and SMAB, with fresh water near the coast driven by freshwater input from various rivers.

3.2. *Comparison between density-based MLDs and temperature-based MLDs*

As an alternative method, we applied a 0.2 °C temperature threshold to detect the MLD in the *in-situ* profiles (Section 2.3). The temperature- and density-based MLDs are generally consistent (Fig. 13). The mean differences between density-based and temperature-based MLD are 4.7 ± 18.4 m (winter), 7.7 ± 23.4 m (spring), 1.8 ± 10.0 (summer), and 5.9 ± 12.5 m (fall), thus not statistically different. Most winter profiles (76%) exhibit differences between density-based and temperature-based MLDs less than 10 m, with 43% showing identical MLDs from the two thresholds. The two methods resulted in identical MLDs in 39% of total profiles in spring, 53% of the profiles in summer, and just 25% of profiles in fall. When the two methods produce different MLDs, the temperature-based MLDs are most often biased deep compared to density-based MLDs, particularly in spring and fall. This suggests that haline effects are driving shallower density-based MLDs (e.g., Christensen and Pringle, 2012).

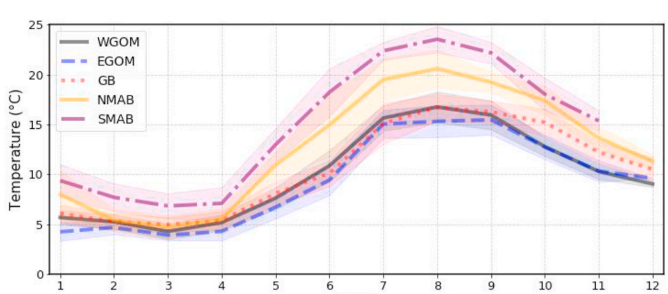

Fig. 9. Mixed layer temperature (MLT) climatological seasonal cycle from *in situ* observations using density threshold-based MLD with the 1 standard deviation (STD) ranges shaded, for each eco-region. The regional mean MLTs are calculated first for each month/year, and monthly means and STDs are calculated subsequently so that the shading primarily reflects interannual variations.

Comparing seasons and eco-regions, the MLDs calculated based on the two methods are consistent overall, but with some seasonal and regional differences (Table 1). The correlations are higher on GB and in the SMAB and NMAB. Correlations are particularly weak in the EGOM in spring and summer ($r = 0.42$ and 0.28, respectively). The root-mean-square-error (RMSE) is lowest in summer in all eco-regions except in the EGOM (RMSE values range from 1.9 m–7.7 m), when the MLDs are generally small.

While the seasonal cycle and spatial distribution of the mean MLDs calculated using the density and temperature criteria are overall consistent, there are some discrepancies worth highlighting. Monthly averaged MLDs within each region show that the temperature-based MLDs are generally biased deep compared to density-based MLDs, as all the monthly mean differences are positive (Fig. 14). These differences are most prominent in spring, particularly in April, and late fall to early winter (although data coverage is very limited in late fall – early winter). In the WGOM, the differences between temperature-based MLDs and density-based MLDs are largest from October to December (5.8 m–32.7 m) and spring (8.8 m–18.8 m) and smallest from June through September (0.6 m–1.4 m). A similar pattern is observed in the EGOM. GB, the NMAB, and the SMAB show smaller differences between the MLDs derived based on the two criteria, with all 3 regions peaking in November or December and April.

Spatially, the greatest positive MLD differences in winter are found near the GB shelf-break as well as in the Great South Channel (Fig. 15). Concentration of large positive MLD differences to the west of Wilkinson Basin in winter is consistent with the earlier findings by Christensen and Pringle (2012) who showed that these are primarily controlled by the haline stratification due to surface freshwater. Similar patterns are observed in spring, but with the addition of large positive MLD differences in the northeastern reaches of the GOM. Additionally, positive MLD differences are found along the SMAB and NMAB shelfbreak. In summer, temperature-based MLDs are deeper than density-based MLDs on GB, with only scattered instances elsewhere. In fall, the large positive MLD differences are primarily distributed around the northern coastal boundary of the EGOM and WGOM, as well as on GB. The relatively fewer large positive differences in winter along the coastal boundary of the GOM seems partly due to the low data coverage (gray background shadings in Fig. 15) in that region.

3.3. *Long-term variability and trends*

In this subsection, we examine the interannual variability and long-term linear trends of MLD in each season across the 5 eco-regions. This analysis is based on the MLD defined using the density method (threshold: 0.03 kg/m^3). Data coverage varies in all seasons across the eco-regions resulting in some data gaps. While we have not found any evidence that the results discussed here are affected by uneven data coverage, they should be interpreted with caution. Here, we consider linear trends having $p \leq 0.15$ to be statistically significant. Overall, interannual variability dominates over linear trends across all regions and seasons. Only seven region-season pairs out of 20 (NMAB winter, EGOM spring, WGOM spring, NMAB summer, WGOM fall, NMAB fall, and GB fall) exhibit statistically significant trends (Fig. 16). Three region-season pairs show a negative MLD trend, −0.32 m/year in EGOM

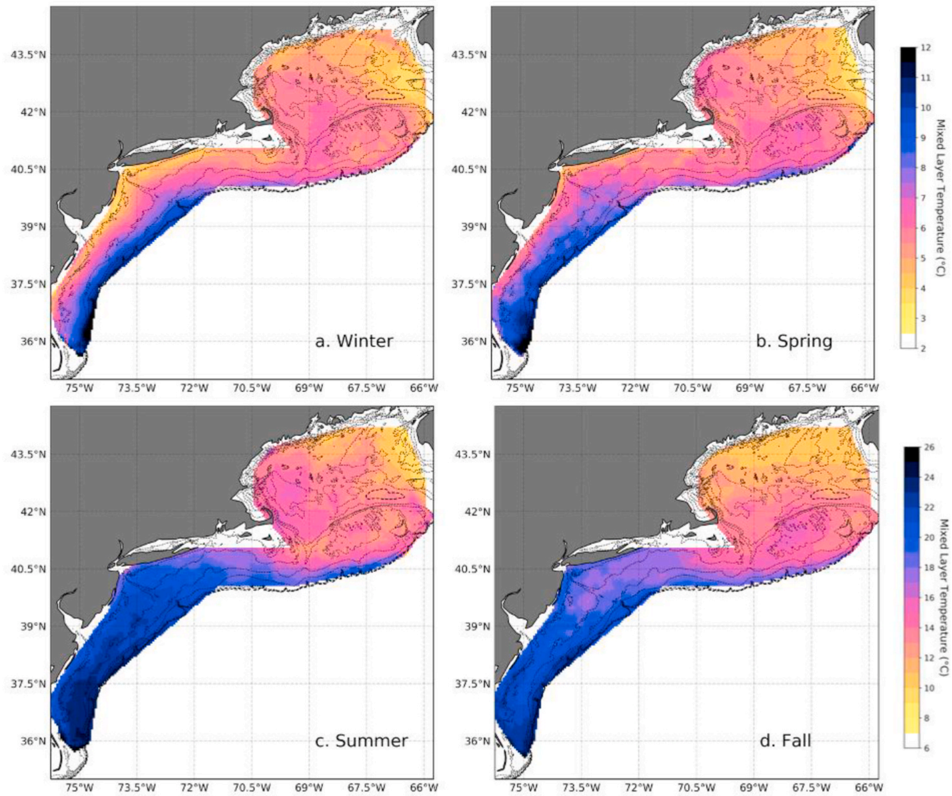

Fig. 10. As in Fig. 7, but for the MLT. Note that the (a–b) and (c–d) use different color ranges.

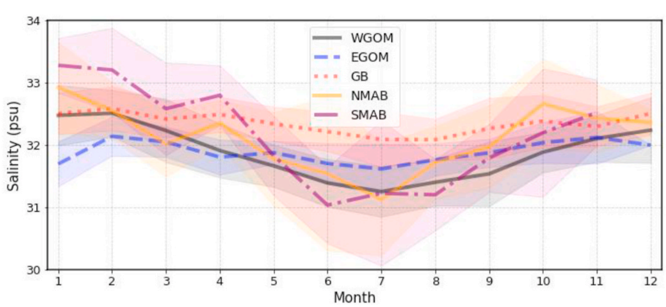

Fig. 11. As in Fig. 9, but for the mixed layer salinity (MLS).

spring, −0.21 m/year in GB fall, and −0.53 m/year in WGOM spring. On the other hand, the other regions show increasing MLD trends ranging from +0.11 m/year in NMAB summer and WGOM fall to +0.46 m/year in NMAB winter. Overall, there is no clear regional or seasonal pattern in long-term trends.

The interannual correlations between regions are calculated to determine how the long-term trends and variability are related among regions (Table 2). The correlations are moderate to weak in general. The strongest correlation across all regions and seasons is found in fall between the WGOM and EGOM (r = 0.69). Correlations between these regions remain relatively high in spring as well (r = 0.60). Generally, the correlations are stronger in fall than spring. Correlations are generally weak in summer, with the exception being the correlation measured between WGOM and the NMAB (r = 0.61). In winter, most cases have fewer than 21 years of data, thus the correlations are not very reliable.

4. Comparison between observational density-based MLDs and GLORYS12V1 MLDs

As the observational data coverage is not sufficient to generate regional MLD time series without gaps, we test whether the MLD provided by GLORYS12V1 is realistic enough to replace observations in our analysis of the long-term variability. The GLORYS12V1 is chosen because it is a global ocean reanalysis with the highest horizontal resolution currently available. In addition, it has been shown to be representative of surface and bottom temperature and salinity on the NEUS continental shelf (Chen et al., 2021). Since the MLD provided by GLORYS12V1 (Section 2.2) is derived using a different method from the one we have applied to the observations (Section 2.3), we compare the density-based MLD from observations with the GLORYS12V1 MLD from two different sources: (1) provided directly by the GLORYS12V1 reanalysis product (GMLD), and (2) calculated by us from GLORYS12V1 temperature and salinity profiles using a density threshold of 0.03 kg/m^3 (GMLD03). The comparison between the two GLORYS12V1 MLDs will highlight the sensitivity to the MLD detection method. Note that both the GMLD and GMLD03 are calculated or subsampled at the time and space points closest to each observation to avoid introducing differences due to spatial variations.

Overall, the correlation between GMLD and GMLD03 is high in all seasons except for the summer (Table 3). While the low correlation in summer is somewhat expected as the error could easily dominate the signal when the variability is weak and the mean is small, a closer inspection reveals that the low correlations in the summer are due to the fact that the GMLDs and GMLD03s are almost uniformly 10 m and 5 m, respectively, with little spatial or temporal variability (not shown). In general, our density threshold criteria result in an unrealistic number of fully stratified profiles (i.e. MLD = 5 m) in GMLD03. For GMLD03, 85.6% of the total GLORYS12V1 profiles in summer are categorized as fully stratified, while 30.9%, 14.3% and 3.0% are fully stratified during spring, fall, and winter, respectively. A similar number of profiles would be similarly categorized in GMLD if we consider anything shallower than 11 m as fully stratified (winter: 9.6%, spring: 59.2%, summer: 96.9%, and fall: 27.8%). For comparison, the observed *in situ* profiles yield, 2.4%, 12.7%, 39.8%, and 10.7% fully stratified profiles for winter,

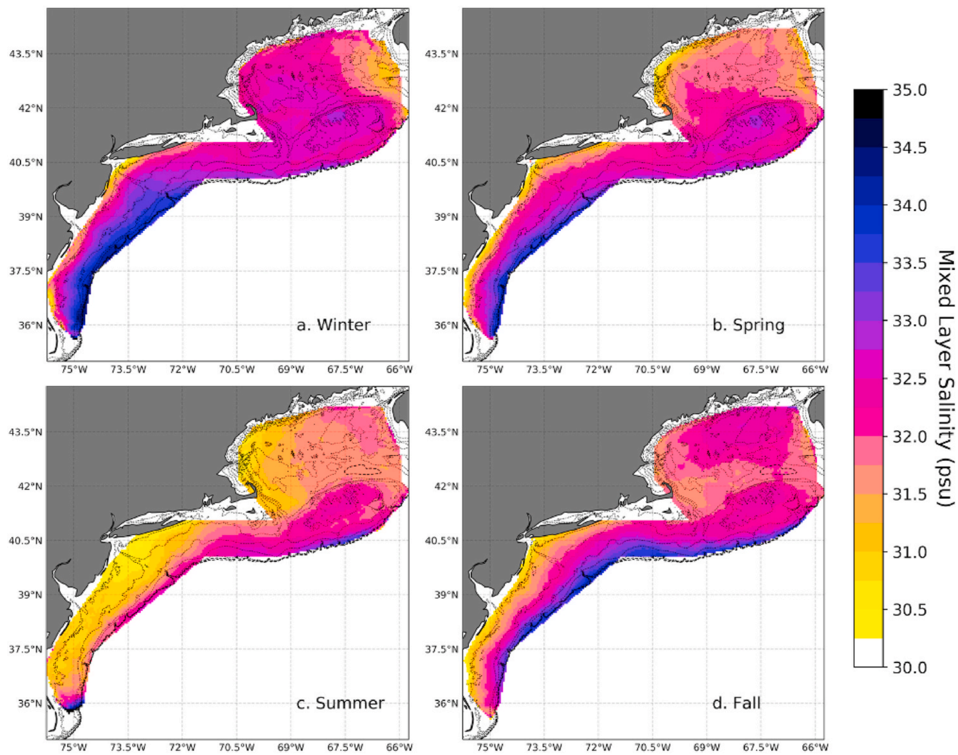

Fig. 12. As in Fig. 7, but for the MLS.

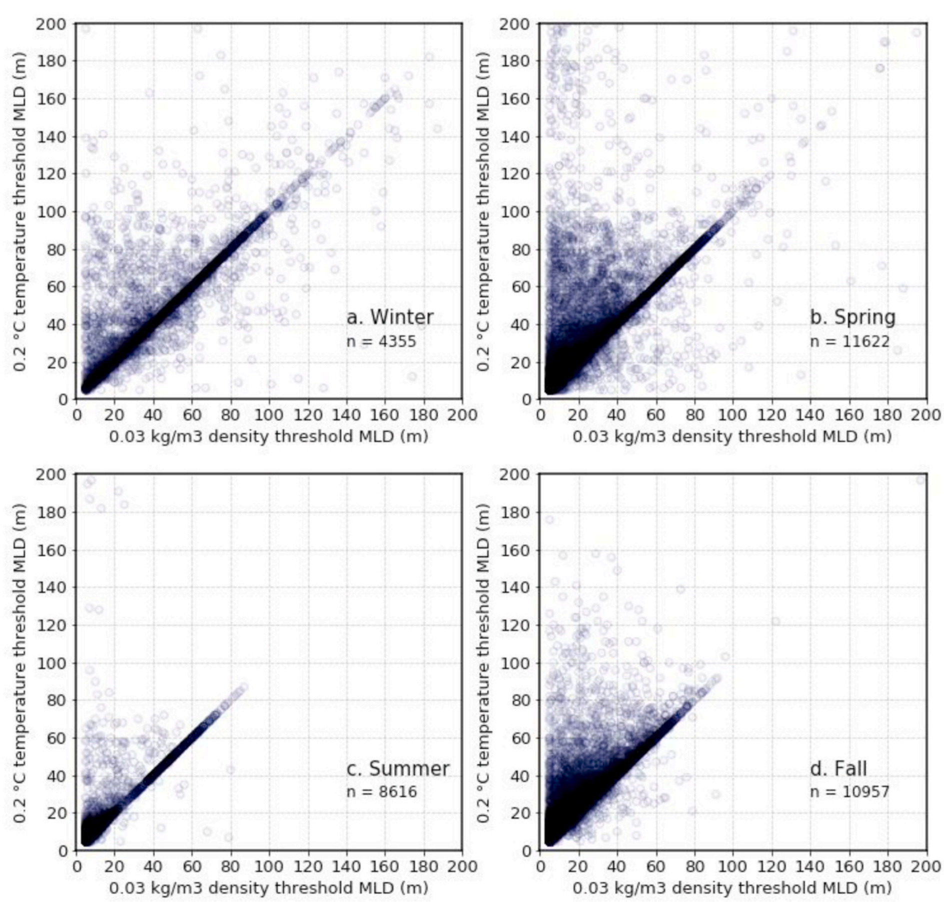

Fig. 13. Comparison of observed MLDs from the density method (threshold: 0.03 kg/m^3) against MLDs from the temperature method (threshold: 0.2 °C) for the entire NEUS continental shelf in each season: **(a)** winter, **(b)** spring, **(c)** summer, and **(d)** fall.

Table 1
Correlations and root-mean-square-error (RMSE; unit: meter) using all data points between the density-based and temperature-based MLDs calculated for 5 eco-regions in each season. All correlation values are significant at the 95% confidence level.

	EGOM		WGOM		GB		NMAB		SMAB	
	r	RMSE	r	RMSE	r	RMSE	r	RMSE	r	RMSE
Winter	0.83	18.4	0.78	28.1	0.76	17.2	0.72	15.1	0.78	17.2
Spring	0.42	33.9	0.48	41.0	0.78	18.0	0.75	14.8	0.76	14.7
Summer	0.28	25.4	0.57	5.9	0.91	7.7	0.89	2.4	0.85	1.9
Fall	0.64	20.2	0.70	16.6	0.81	12.8	0.79	10.2	0.77	8.6

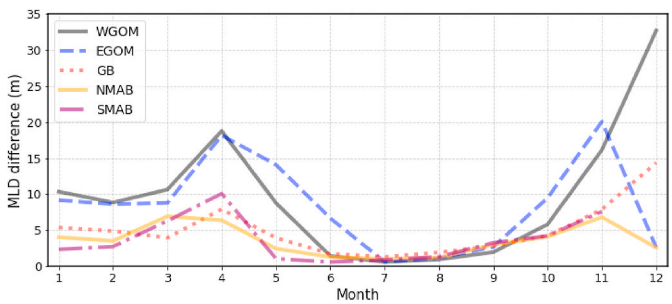

Fig. 14. Spatially averaged and climatological MLD difference (temperature-based MLDs minus density-based MLDs) for the 5 eco-regions in each month. The MLD differences are calculated from regional mean MLDs which are calculated first for each month/year. Note that there are only 247 profiles from 4 years (1993, 1994, 2010, and 2011) in December.

spring, summer, and fall, respectively.

The correlations between observation-based MLDs and GMLDs are only moderate (but significant) in all seasons except summer (*r* ranging from 0.48 in GB/spring to 0.86 in GB/fall; Table 3). This is also true for GMLD03 compared with observational density-based MLDs. Since the GMLD and GMLD03 are highly correlated with each other, the relatively weak correlations with observational MLDs cannot be attributed to differences arising from the detection method. The lack of variability in GMLD and GMLD03 in summer results in particularly poor correlations with observations, except in the NMAB.

Next, we compare the mean MLDs in each season and region (Table 4). Overall, the mean values from the GMLD and GMLD03 compare favorably with the observed values, unlike the interannual correlations. Note that the threshold for GMLD in January–April is smaller than the 0.03 kg/m^3 threshold applied to the observations (Fig. 3). This suggests that the more generous threshold resulted in deeper MLDs, which is also consistent with the fact that the GMLD03 compares more favorably with observations for the most regions in winter and spring. The mean summer GMLD, GMLD03, and observation-based MLD values have a narrow range, consistent with the large number of fully stratified profiles, in particular for the GMLD. In fall, the GMLD is slightly more consistent with the observation than GMLD03.

On average, the largest differences in GMLD and observational MLDs within each region are in winter and spring (Fig. 17). The region with the greatest overall difference is GB, likely related to the fact the ocean model for the GLORYS12V1 does not include tidal mixing, while the other regions show a similar shape with similar magnitudes. Unlike the difference between GMLD and observational density-based MLDs, the differences between GMLD03 and observational density-based MLDs are positive in winter (GMLD03 MLDs are deeper than the latter), except in the NMAB. From April to August, the difference in most regions is

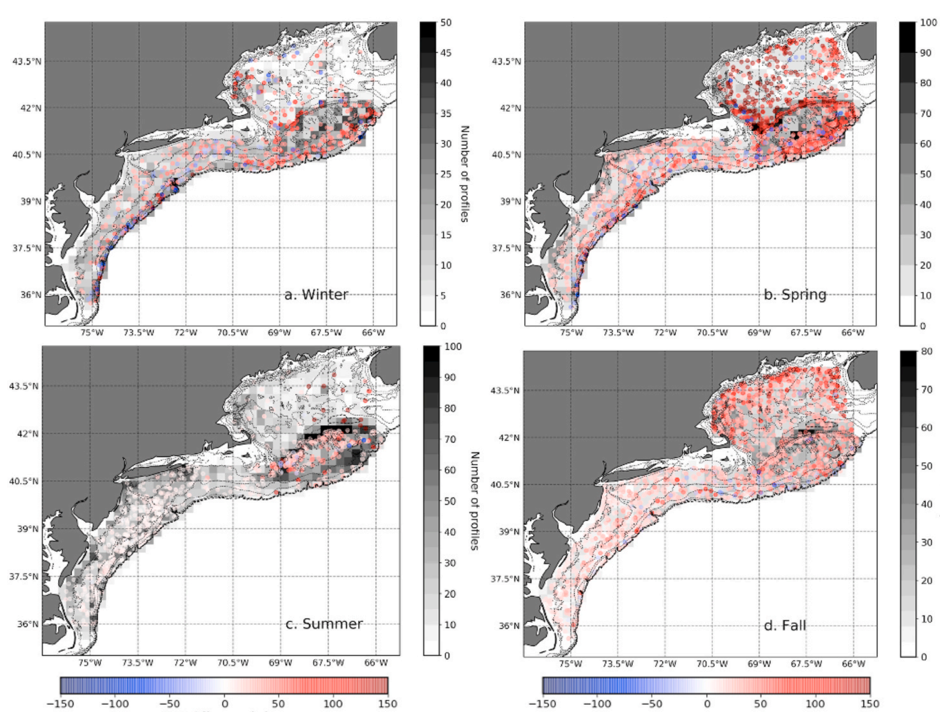

Fig. 15. Locations where the difference between the two methods (temperature-based MLD minus density-based MLD) is greater than 1 standard deviations from zero difference, shown for each season: **(a)** winter, **(b)** spring, **(c)** summer, and **(d)** fall. The magnitude of differences are shown by the colored dots, while the gray shading indicates data availability for each 0.25° × 0.25° bin.

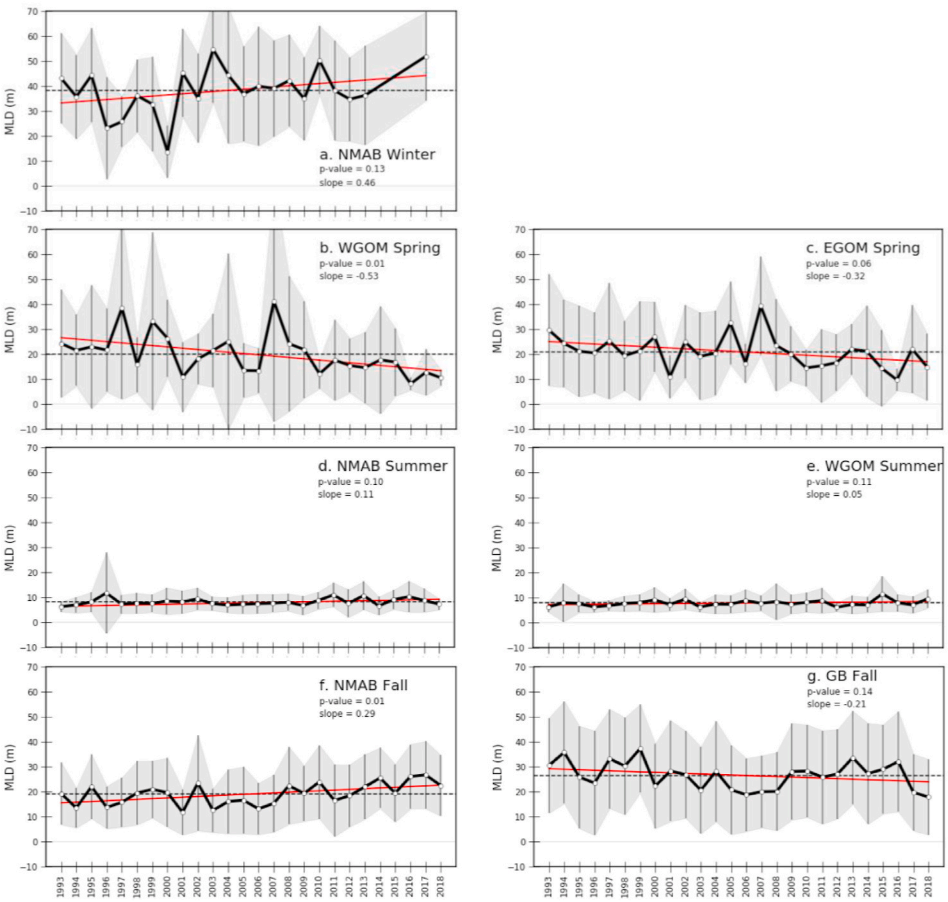

Fig. 16. MLD timeseries from 1993 to 2018 shown for eco-regions **(a)** NMAB winter, **(b)** WGOM spring, **(c)** EGOM spring, **(d)** NMAB summer, **(e)** WGOM summer, **(f)** NMAB fall, and **(g)** GB fall with trends that are statistically significant (i.e., $p \leq 0.15$). The linear trend is illustrated using a red solid line while the long-term average is shown using a black dashed line. The value of long-term linear trend (m/year) is indicated in each panel along with corresponding p-value. 1 STD is shown using shading.

Table 2

Interannual correlation of MLDs between eco-regions. Note that the linear trends are removed from each time series prior to calculating the correlations. Statistically significant correlations ($p \leq 0.10$) are in yellow shaded boxes. Statistically significant correlations ($p \leq 0.15$) are indicated using asterisks. Correlation calculations using fewer than 21 years of data are indicated with gray font.

Winter	EGOM	WGOM	GB	NMAB	SMAB
EGOM					
WGOM	0.17				
GB	0.05	0.14			
NMAB	-0.57	0.30	0.58		
SMAB	-0.15	0.34	-0.29	-0.05	

Spring	EGOM	WGOM	GB	NMAB	SMAB
EGOM					
WGOM	0.60				
GB	0.17	-0.07			
NMAB	-0.29	-0.10	0.24		
SMAB	0.59	0.24	0.20	0.07	

Summer	EGOM	WGOM	GB	NMAB	SMAB
EGOM					
WGOM	0.28				
GB	0.30*	0.43			
NMAB	0.08	0.61	0.13		
SMAB	0.17	-0.01	0.12	0.03	

Fall	EGOM	WGOM	GB	NMAB	SMAB
EGOM					
WGOM	0.69				
GB	0.43	0.57			
NMAB	0.27	0.38	-0.01		
SMAB	0.27	0.03	-0.21	0.53	

slightly negative. In fall, GMLD03 MLDs are generally deeper than observational density-based MLDs.

5. Discussion and summary

A description of the density-based MLD seasonal cycle has been constructed for the NEUS continental shelf based on *in situ* observations. In addition, the observed MLDs are compared to GLORYS12V1 MLDs as well as the recalculated density-based MLDs from corresponding temperature and salinity profiles in GLORYS12V1. The MLD climatological seasonal cycle for the 5 eco-regions show important regional differences in amplitude, where the seasonal cycle is weakest on GB and in the SMAB regions and strongest in the WGOM. The observational density-based MLD climatology is useful as a baseline for future studies of MLD changes and their drivers in the study region. The MLD definition used in this study, however, is not without caveats (e.g., the upper limit of the surface layer could have been defined at 6 m or 10 m instead of 5 m). Despite these limitations, this study presents a MLD climatology for the NEUS continental shelf at a higher horizontal resolution than existing global MLD climatologies.

An important limitation to interpreting our results is that the observational data is distributed unevenly in time and space. We

Table 3
Interannual correlation between MLDs provided by GLORYS12V1 (GML) or recalculated using GLORYS12V1 density profiles (GMLD03), and observational density-based MLD (obsMLD03). Note that the correlation values are calculated from seasonal means and the linear trends are removed from each time series prior to calculating the correlations. Values that are statistically significant at $p < 0.10$ are indicated with asterisks. Gray shading indicates that fewer than 21 years of observational data was used.

		GMLD & GMLD03	GMLD & ObsMLD03	GMLD03 & ObsMLD03
Winter	EGOM	0.98*	0.73*	0.73*
	WGOM	0.92*	0.76*	0.74*
	GB	0.91*	0.63*	0.60*
	NMAB	0.86*	0.68*	0.66*
	SMAB	0.95*	0.65*	0.60*
Spring	EGOM	0.90*	0.62*	0.60*
	WGOM	0.89*	0.76*	0.86*
	GB	0.79*	0.48*	0.73*
	NMAB	0.85*	0.73*	0.81*
	SMAB	0.90*	0.81*	0.71*
Summer	EGOM	0.51*	0.19	0.61*
	WGOM	0.40*	0.33	0.41*
	GB	0.71*	0.07	0.22
	NMAB	0.59*	0.65*	0.93*
	SMAB	0.82*	0.17	0.10
Fall	EGOM	0.98*	0.82*	0.81*
	WGOM	0.98*	0.76*	0.76*
	GB	0.95*	0.86*	0.91*
	NMAB	0.95*	0.75*	0.68*
	SMAB	0.86*	0.60*	0.67*

Table 4
Spatially averaged mean MLDs and their standard deviations (STDs) by season and region (in meters). The regional mean MLDs are calculated first for each season/year, and seasonal means and STDs are calculated subsequently so that the STDs primarily reflects interannual variations.

		ObsMLD03	GMLD	GMLD03
Winter	EGOM	41.1 ± 12.7	40.0 ± 14.5	49.7 ± 18.3
	WGOM	73.4 ± 23.2	61.4 ± 20.63	79.9 ± 21.1
	GB	44.5 ± 9.4	39.1 ± 9.2	49.0 ± 8.3
	NMAB	38.3 ± 9.5	29.5 ± 7.8	38.6 ± 7.7
	SMAB	36.0 ± 6.9	29.9 ± 5.9	39.8 ± 8.2
Spring	EGOM	21.2 ± 6.3	15.9 ± 4.0	22.9 ± 7.5
	WGOM	19.7 ± 8.5	14.3 ± 4.1	19.5 ± 7.6
	GB	31.9 ± 6.7	17.4 ± 3.9	25.3 ± 7.2
	NMAB	21.7 ± 5.7	15.1 ± 4.3	18.9 ± 5.6
	SMAB	19.4 ± 4.6	16.0 ± 2.7	19.3 ± 4.9
Summer	EGOM	8.3 ± 1.8	10.6 ± 0.2	7.5 ± 1.8
	WGOM	7.8 ± 1.2	10.6 ± 0.1	5.7 ± 0.8
	GB	14.1 ± 2.5	10.6 ± 0.1	6.8 ± 1.1
	NMAB	7.9 ± 2.7	10.6 ± 0.1	6.0 ± 2.1
	SMAB	7.1 ± 1.0	10.6 ± 0.2	6.0 ± 2.1
Fall	EGOM	22.1 ± 5.4	23.8 ± 6.0	29.3 ± 6.9
	WGOM	22.7 ± 5.2	22.5 ± 5.5	27.3 ± 6.0
	GB	26.6 ± 5.3	24.0 ± 5.6	30.5 ± 6.9
	NMAB	18.9 ± 4.0	16.8 ± 2.9	19.1 ± 3.9
	SMAB	13.2 ± 3.2	14.2 ± 2.3	15.2 ± 4.1

compared observational MLDs with GLORYS12V1 to determine whether GLORYS12V1 sufficiently reproduces observational MLDs. The mean MLD values for each season and region from GLORYS12V1 compare reasonably with observations, especially once differences in the MLD definitions are accounted for. Interannual MLD variability in GLORYS12V1 is modestly (but significantly) correlated with observations ($r = \sim 0.5$–0.8), except for some regions during summer where correlations are insignificant. This contrasts with the consistently high correlations ($r > 0.96$) reported across all regions between GLORYS12V1 sea surface temperatures and observations (Chen et al., 2021). Differences in the interannual variability of MLD as measured by observations and in GLORYS12V1 are significant enough to preclude further investigation of long-term MLD variations using the reanalysis. In particular, the stratification in the reanalysis seems overly strong, resulting in an unrealistic

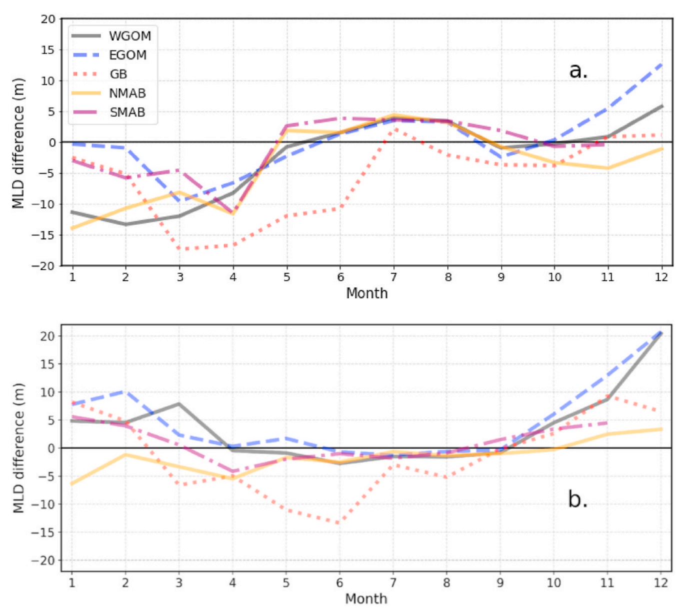

Fig. 17. Spatially averaged and climatological MLD difference of **(a)** GMLD minus observational density based MLDs and **(b)** GMLD03 minus observational density-based MLDs for the 5 eco-regions.

number of fully-stratified profiles particularly in summer. The modest performance of the reanalysis in terms of MLD, is perhaps not surprising since the MLD is not a directly assimilated variable, thereby posing a greater challenge for the reanalysis. Our result suggests that a more systematic assessment of multiple reanalysis products against observations from the NEUS coastal environment is needed in the future. Comparisons with reanalysis products have a practical value as these products are increasingly used, often replacing observational products. For example, the NEFSC State of the Ecosystem Report has constructed indices using the reanalysis products because they often offer better spatial and temporal coverage than the raw observations.

Further investigation into potential drivers of MLD variability is warranted, including surface meteorological variables like wind speed and air temperature. Future directions of study might include an investigation of long-term SST trends and variability as they relate to this MLD dataset. Specifically, whether SST variability is driven by MLD variability and whether SST warms faster in regions where the MLD is shoaling (as indicated by our observed MLD in three region-season pairs) or vice versa. Also, the relationship between the upper ocean stratification variability (Li et al., 2015; Harden et al., 2020) and MLD variability should be further investigated. In addition, questions remain regarding the influence of MLD variability on changes in the upper ocean heat content. Results such as these can be used to inform calculations of ocean heat content, improving on estimations using the whole water column. Finally, because MLD determines the upper ocean heat capacity, from which atmospheric storms derive energy, investigations such as this one may lead to advances in understanding trends in storm intensity and persistence.

Data sets

This study has been conducted using E.U. Copernicus Marine Service Information. GLORYS12V1 data are available from Copernicus Marine Environment Monitoring Service at: https://resources.marine.copernicus.eu/?option=com_csw&view=details&product_id=GLOBAL_REANALYSIS_PHY_001_030. NEFSC data are publicly available from the World Ocean Database maintained by NOAA's National Centers for Environmental Information at: http://www.nodc.noaa.gov/OC5/SELECT/dbsearch/dbsearch.html.

Declaration of competing interest

The authors declare that they have no known competing financial interests or personal relationships that could have appeared to influence the work reported in this paper.

Acknowledgements

The authors gratefully acknowledge the constructive reviews by the two anonymous reviewers and the editor Dr. Arnoldo Valle-Levinson, and the support from the NOAA Modeling, Analysis, Predictions, and Projections (MAPP) Program (NA17OAR4310111) and Climate Variability and Predictability Program (NA20OAR4310482). Cassia Cai acknowledges the Woods Hole Oceanographic Institution Summer Student Fellowship program for participation, the Northwestern University (NU) Earth and Planetary Science Independent Study for supporting the writing of this manuscript, and the NU Climate Change Research Group for providing some of the technical tools to conduct analysis. We also appreciate the free availability of the GLORYS12V1 dataset from the Copernicus Marine Environment Monitoring Service.

References

Alexander, M.A., Scott, J.D., Deser, C., 2000. Processes that influence sea surface temperature and ocean mixed layer depth variability in a coupled model. J. Geophys. Res.: Oceans 105 (1978–2012), 16823–16842. https://doi.org/10.1029/2000JC900074.

Alexander, M.A., Scott, J.D., Friedland, K.D., Mills, K.E., Nye, J.A., Pershing, A.J., Thomas, A.C., 2018. Projected sea surface temperatures over the 21st century: changes in the mean, variability and extremes for large marine ecosystem regions of Northern Oceans. Elem. Sci. Anth. 6 https://doi.org/10.1525/elementa.191.

Amante, C., Eakins, B.W., 2009. ETOPO1 1 Arc-Minute Global Relief Model: Procedures, Data Sources and Analysis, vol. 24. NOAA Technical Memorandum NESDIS NGDC, p. 19.

Bisagni, J.J., Kim, H.-S., Chaudhuri, A., 2016. Interannual variability of the shelf-slope front position between 75° and 50° W. J. Mar. Syst. 78, 337–350.

Brown, W.S., Beardsley, R.C., 1978. Winter circulation in the western Gulf of Maine: Part 1. Cooling and water mass formation. J. Phys. Oceanogr. 8, 265–277.

Chen, K., Gawarkiewicz, G., Lentz, S.J., Bane, J.M., 2014. Diagnosing the warming of the Northeastern U.S. Coastal Ocean in 2012: a linkage between the atmospheric jet stream variability and ocean response. J. Geophys. Res. Oceans 119, 218–227. https://doi.org/10.1002/2013JC009393.

Chen, K., Gawarkiewicz, G., Kwon, Y.-O., Zhang, W.G., 2015. The role of atmospheric forcing versus ocean advection during the extreme warming of the Northeast U.S. continental shelf in 2012. J. Geophys. Res. Oceans 120, 4324–4339. https://doi.org/10.1002/2014JC010547.

Chen, K., Kwon, Y.-O., 2018. Does pacific variability influence the Northwest atlantic shelf temperature? J. Geophys. Res. 123 https://doi.org/10.1029/2017JC013414.

Chen, Z., Kwon, Y.-O., Chen, K., Fratantoni, P., Gawarkiewicz, G., Joyce, T., 2020. Long-term SST variability over the Northwest atlantic continental shelf and slope. Geophys. Res. Lett. 47, e2019GL085455.

Chen, Z., Kwon, Y.-O., Chen, K., Fratantoni, P., Gawarkiewicz, G., Joyce, T.J., Miller, T. J., Nye, J.A., Saba, V.S., Stock, B.C., 2021. Seasonal prediction of bottom temperature on the northeast U.S. Continental shelf. J. Geophys. Res. https://doi.org/10.1029/2021JC017187.

Christensen, M.K., Pringle, J.M., 2012. The frequency and cause of shallow winter mixed layers in the Gulf of Maine. J. Geophys. Res. 117 https://doi.org/10.1029/2011JC007358.

de Boyer Montegut, C., 2004. Mixed layer depth over the global ocean: an examination of profile data and a profile-based climatology. J. Geophys. Res. 109, 1521–1620. https://doi.org/10.1029/2004JC002378.

Drillet, Y., Lellouche, J.M., Levier, B., Drévillon, M., Le Galloudec, O., Reffray, G., Regnier, C., Greiner, E., Clavier, M., 2014. Forecasting the mixed-layer depth in the Northeast Atlantic: an ensemble approach, with uncertainties based on data from operational ocean forecasting systems. Ocean Sci. 10, 1013–1029.

Fernandez, E., Lellouche, J.M., 2018. Product user manual for the global ocean physical reanalysis product GLORYS12V1. Copernicus Product User Manual 4, 1–15.

Forsyth, J., Andres, M., Gawarkiewicz, G.G., 2015. Recent accelerated warming of the continental shelf off New Jersey: observations from the CMVOleander expendable bathythermograph line. J. Geophys. Res. 120, 2370–2384.

Fratantoni, P.S., Pickart, R.S., 2007. The western north atlantic shelfbreak current system in summer. J. Phys. Oceanogr. 37, 2509–2533. https://doi.org/10.1175/JPO3123.1.

Fratantoni, P.S., Holzwarth-Davis, T., Melrose, D.C., Taylor, M.H., 2019. Description of Oceanographic Conditions on the Northeast US Continental Shelf during 2016. US Dept. Commer., Northeast Fish Sci Cent Ref Doc, p. 39, 19-07. http://www.nefsc.noaa.gov/publications/.

Gawarkiewicz, G.G., Todd, R.E., Plueddemann, A.J., Andres, M., Manning, J.P., 2012. Direct interaction between the Gulf stream and the shelfbreak south of new England. Sci. Rep. 2, 1–6.

Gawarkiewicz, G., Chen, K., Forsyth, J., Bahr, F., Mercer, A.M., 2019. Characteristics of an advective marine heatwave in the middle atlantic Bight in early 2017. Front. Mar. Sci. 6 https://doi.org/10.3389/fmars.2019.00712.

Greene, C.H., Meyer-Gutbrod, E., Monger, B.C., McGarry, L.P., Pershing, A.J., Belkin, I. M., Fratantoni, P.S., Mountain, D.G., Pickart, R.S., Proshutinsky, A., Ji, R., Bisagni, J. J., Hakkinen, S.M.A., Haidvogel, D.B., Wang, J., Head, E., Smith, P., Reid, P.C., Conversi, A., 2013. Remote climate forcing of decadal-scale regime shifts in Northwest Atlantic shelf ecosystems. Limnol. Oceanogr. 58, 803–816.

Harden, B.E., Gawarkiewicz, G.G., Infante, M., 2020. Trends in physical properties at the southern New England shelf break. J. Geophys. Res.: Oceans 125. https://doi.org/10.1029/2019JC015784.

Holte, J., Talley, L., 2009. A new algorithm for finding mixed layer depths with applications to argo data and subantarctic mode water formation. J. Atmos. Ocean. Technol. 26, 1920–1939. https://doi.org/10.1175/2009JTECHO543.1.

Lellouche, J.M., Greiner, E., Le Galloudec, O., Garric, G., Regnier, C., Drevillon, M., Benkiran, M., Testut, C.-M., Bourdalle-Badie, R., Gasparin, F., Hernandez, O., Levier, B., Drillet, Y., Remy, E., Le Traon, P.-Y., 2018. Recent updates to the Copernicus Marine Service global ocean monitoring and forecasting real-time 1/ 12° high-resolution system. Ocean Sci. 14, 1093–1126.

Li, Y., Fratantoni, P.S., Chen, C., Hare, J.A., Sun, Y., Beardsley, R.C., Ji, R., 2015. Spatio-temporal patterns of stratification on the Northwestern Atlantic shelf. Prog. Oceanogr. 134, 123–137.

Loder, J.W., Drinkwater, K.F., Hannah, C.G., Greenberg, D.A., Smith, P.C., 1993. Circulation, hydrographic structure and mixing at tidal fronts: the view from Georges Bank. Philos. Trans. R. Soc. London, Ser. A 343, 447–460.

Loder, J.W., Petrie, B., Gawarkiewicz, G., 1998. The coastal ocean off north-eastern North America: a large-scale view. Sea 11, 105–133.

Mills, K.E., Pershing, A.J., Brown, C.J., Chen, Y., Chiang, F.-S., Holland, D.S., Lehuta, S., Nye, J.A., Sun, J.C., Thomas, A.C., Wahle, R.A., 2013. Fisheries management in a changing climate: lessons from the 2012 ocean heat wave in the Northwest atlantic. Oceanog 26, 1–6. https://doi.org/10.5670/oceanog.2013.27.

Mountain, D.G., Jessen, P.F., 1987. Bottom waters of the Gulf of Maine, 1978-1983. J. Mar. Res. 45, 319–345.

Mountain, D.G., Manning, J.P., 1994. Seasonal and interannual variability in the properties of the surface waters of the Gulf of Maine. Continent. Shelf Res. 14, 1555–1581.

Mountain, D.G., Taylor, M.H., 1998. Spatial coherence of interannual variability in water properties on the U.S. northeast shelf. J. Geophys. Res.: Oceans 103, 3083–3092. https://doi.org/10.1029/97JC03052.

Mountain, D.G., 2012. Labrador slope water entering the Gulf of Maine—response to the north atlantic oscillation. Continent. Shelf Res. 47, 150–155. https://doi.org/10.1016/j.csr.2012.07.008.

Niiler, P.P., 1975. Deepening of the wind-mixed layer. J. Mar. Res. 33, 405–422.

Nye, J.A., Link, J.S., Hare, J.A., Overholtz, W.J., 2009. Changing spatial distribution of fish stocks in relation to climate and population size on the Northeast United States continental shelf. Mar. Ecol. Prog. Ser. 393, 111–129.

Nye, J.A., Joyce, T.M., Kwon, Y.-O., Link, J.S., 2011. Gulf Stream position determines spatial distribution of silver hake. Nat. Commun. 2, 412. https://doi.org/10.1038/ncomms1420.

Pershing, A.J., Alexander, M.A., Hernandez, C.M., Kerr, L.A., Le Bris, A., Mills, K.E., Nye, J.A., Record, N.R., Scannell, H.A., Scott, J.D., Sherwood, G.D., Thomas, A.C., 2015. Slow adaptation in the face of rapid warming leads to the collapse of atlantic Cod in the Gulf of Maine. Science. https://doi.org/10.1126/science.aac9819.

Richaud, B., Kwon, Y.-O., Joyce, T.M., Fratantoni, P.S., Lentz, S.J., 2016. Surface and bottom temperature and salinity climatology along the continental shelf off the Canadian and U.S. East Coasts. Continent. Shelf Res. 124, 165–181.

Shearman, R.K., Lentz, S.J., 2010. Long-term sea surface temperature variability along the U.S. East coast. J. Phys. Oceanogr. 40, 1004–1017.

Taylor, M.H., Mountain, D.G., 2009. The influence of surface layer salinity on wintertime convection in Wilkinson Basin, Gulf of Maine. Cont. Shelf Res. 29, 433–444. https://doi.org/10.1016/j.csr.2008.11.002.

Thomson, R., Fine, I., 2003. Estimating mixed layer depth from oceanic profile data. J. Atmos. Ocean. Technol. 20, 319–329.

Townsend, D.W., Thomas, A.C., Mayer, L.M., Quinlan, J.A., 2006. Oceanography of the northwest Atlantic continental shelf. Sea 14A, 119–168.

Vermersch, J.A., Beardsley, R.C., Brown, W.S., 1979. Winter circulation in the western Gulf of Maine Part 2. Current and pressure observations. J. Phys. Oceanogr. 9, 768–784.

Yamamoto, A., Tatebe, H., Nonaka, M., 2020. On the emergence of the atlantic multidecadal SST signal: a key role of the mixed layer depth variability driven by north atlantic oscillation. J. Clim. 33, 3511–3531. https://doi.org/10.1175/JCLI-D-19-0283.1.